

Analyst

Accepted Manuscript



This is an *Accepted Manuscript*, which has been through the Royal Society of Chemistry peer review process and has been accepted for publication.

Accepted Manuscripts are published online shortly after acceptance, before technical editing, formatting and proof reading. Using this free service, authors can make their results available to the community, in citable form, before we publish the edited article. We will replace this *Accepted Manuscript* with the edited and formatted *Advance Article* as soon as it is available.

You can find more information about *Accepted Manuscripts* in the [Information for Authors](#).

Please note that technical editing may introduce minor changes to the text and/or graphics, which may alter content. The journal's standard [Terms & Conditions](#) and the [Ethical guidelines](#) still apply. In no event shall the Royal Society of Chemistry be held responsible for any errors or omissions in this *Accepted Manuscript* or any consequences arising from the use of any information it contains.

ARTICLE

Excellent graphitic carbon nitride nanosheets-based photoelectrochemical platform motivated by Schottky barrier and LSPR effect and its sensing application

Cite this: DOI: 10.1039/x0xx00000x

Hong Dai,^a Shupeizhang,^a Yilin Li^a and Yanyu Lin^{a,b}Received 00th January 2012,
Accepted 00th January 2012

DOI: 10.1039/x0xx00000x

www.rsc.org/

A visible light responsive photocatalytic hybrid with excellent photoelectrochemical activity was firstly fabricated via self-assembly of Au nanorods onto poly(L-cysteine) modified graphitic carbon nitride nanosheets. Herein, layered structural graphitic carbon nitride nanosheets with proper band gap, high stability, and nontoxicity as a photoactive material demonstrate a high photocatalytic activity. Furthermore, the incorporation of multifunctional Au nanorods made the hybrid possesses a Schottky barrier and localized surface plasmonic resonance, which considerably enhanced the separation of the photo-excited electrons and holes, resulting in increased photoelectrochemical performance. As a proof of concept, mercapto-beta-cyclodextrin as a bionic recognition device was introduced into the hybrid to selectively detect naringin on the basis of the dramatic decreasing of photocurrent. The visible-light driven photoelectrochemical sensor exhibited excellent analytical performance including high sensitivity, good selectivity and wide linear range from 1×10^{-4} to 1×10^{-10} M.

Introduction

The dramatically developed and promising photoelectrochemical (PEC) detection has drawn growing research scrutiny in the analytical field for its inexpensive photoelectric devices, high sensitivity and good analytical performance.¹⁻⁴ Heretofore, a series of PEC sensors have been proposed by using wide band-gap semiconductors as photoactive materials.⁵⁻⁶ To better use the visible range of sunlight, novel and promising visible-light-driven photocatalyst is urgently needed to extend.

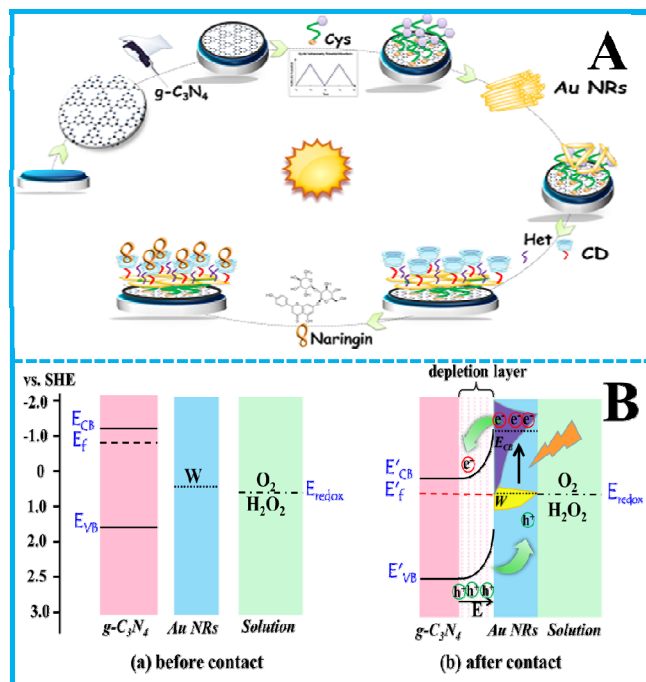
Very recently, an organic and metal-free polymeric photocatalyst, graphitic carbon nitride (g-C₃N₄) is a hot topic. The tri-s-triazine ring structure and high degree of condensation make g-C₃N₄ own high stability with respect to chemical attacks and thermal. Besides, an appealing electronic structure and a medium-gap (2.7 eV) of g-C₃N₄ make it being an outstanding photocatalyst with visible light irradiation ($\lambda < 460$ nm). Therefore, g-C₃N₄ has attracted increasing attention in applications such as catalytic supports, sensing, photocatalysis and electrocatalysis owing to its fascinating properties.⁷⁻¹³ However, the efficiency for bare g-C₃N₄ is still limited due to its fast recombination of photogenerated electron-hole pairs.¹⁴

To date, extensive efforts have been devoted to improving its photocatalytic performance.¹⁵⁻¹⁷ Hereinto, the incorporation of noble metal nanoparticles into semiconductors has drawn great interest recently because the hybrids not only possess the unique properties of semiconductors and noble metals, but also own novel optical, electrical, and catalytic features.¹⁸⁻²³ Surprisingly, although the semiconductor-metal nanomaterials have exhibited excellent photocatalytic performance across the UV-visible region, scarcely

any previous works on that the noble metal was loaded on g-C₃N₄ as a photocatalyst.²⁴ Inspired of this, the Au nanorods (Au NRs) decorated g-C₃N₄ hybrid as an excellent photocatalyst was firstly constructed in this work. The hybrid demonstrated excellent photocatalytic activity due to the synergic effect of Schottky barrier and the localized surface plasmon resonance (LSPR) effect derived from the attachment of Au NRs to g-C₃N₄.²⁵ The Schottky barrier drives the photo-generated electrons and holes to move to different directions, effectively suppressing the recombination of electron-hole pairs. Furthermore, LSPR effect enhances the incident light absorption ability and forced a collective oscillation of the electrons, exciting more electrons and holes. Therefore, the synergic effect between the Schottky barrier and LSPR in the hybrid significantly prompted the visible-light photocatalytic activity of bare g-C₃N₄ making the hybrid a superior signal amplify strategy to fabricate some highly sensitive PEC sensors via linking some modifiers in virtue of the Au-S bond.

To assess the application of the new hybrid in PEC field, an effective, sensitive and specific PEC sensing strategy of Au NRs decorated g-C₃N₄ and mercapto-beta-cyclodextrin (CD) was developed. The sensor can be successfully used to selectively probe Naringin (NA) through reduced photocurrent response due to the specific recognition between CD and NA and presented charming performances. Furthermore, the utilization of zero potential and visible light in this detection largely reduced the interference from other reductive species and avoided inactivation of UV light to biomolecules, respectively, enriching the types of PEC sensor and broadening the application in PEC biosensing. Promisingly, the successful fabrication and application of the hybrid can serve as

guidance for rational construction of highly efficient PEC sensing platform.



Scheme 1 (A) Schematic illustrates the fabrication procedure of the photoelectrochemical sensor. (B) Energy diagrams of the $g\text{-C}_3\text{N}_4$ and Au NRs before (a) and after (b) contact.

Experimental

Materials and Reagents

Melamine, silver nitrate (AgNO_3), L-ascorbic acid (AA), L-cysteine, 4-Aminothiophenol, 4-Mercaptobenzoic, hydrogen tetrachloroaurate trihydrate ($\text{HAuCl}_4 \cdot 3\text{H}_2\text{O}$), cetyltrimethylammonium bromide (CTAB), sodium borohydride (NaBH_4), Naringin, hesperidin and naringin dihydrochalcone (Nadc) were purchased from Sigma-Aldrich (USA) and used without further purification. Hydrogen peroxide (30%), n-Hexadecanethiol (Het), p-Mercaptobenzoic acid (Mba), p-Aminothiophenol (Amt) and CD were obtained from Sinopham Chemical Reagent Co. (Shanghai, China), Hong Rui Kang Reagent Co. (Wuhan, China), and Zhiyuan Bio-Technology Co. (Shandong, China), respectively. The phosphate buffer solution (PBS, 0.1 M, pH 7.0) as the supporting electrolyte was prepared by mixing stock solution of 0.1 M NaH_2PO_4 and 0.1 M Na_2HPO_4 and adjusting the pH. Other reagents were of analytical reagent grade. The water used for the preparation of the solution was purified using a Water purifier (China) purification system.

Construction of Modified Electrodes

Prior to modification, the bare glassy carbon electrode (GCE, $\varphi=3$ mm) was polished with 0.3 and 0.05 μm alumina slurry on chamois leather to produce a mirror-like surface, then washed successively with anhydrous alcohol and doubly distilled water in an ultrasonic bath and dried in air before use. With a micropipette, 4 μL of 3 mg mL^{-1} $g\text{-C}_3\text{N}_4$ solution was dipped on the fresh prepared GCE surface, and then the $g\text{-C}_3\text{N}_4$ modified electrode was obtained after dried under infrared lamp.

The $g\text{-C}_3\text{N}_4/\text{Cys}$ modified electrode was obtained through in situ electrochemical polymerization in 0.1 M of pH 7.0 PBS containing 0.01 M of L-cysteine between -0.2 V and 2.0 V. Then thoroughly washed with redistilled water to remove any physically absorbed material and dried in air. Following that, the modified electrode was immersed into a centrifuge tube containing 100 μL of stock Au NRs solution for 20 min at room temperature and then the $g\text{-C}_3\text{N}_4/\text{Cys}/\text{Au NRs}$ modified electrode was successfully fabricated (Scheme 1). Similarly, the $g\text{-C}_3\text{N}_4/\text{Au NRs}$ modified electrode was successfully developed by the above stepwise without the electropolymerization.

Design of the visible light driven PEC sensor for the detection of NA

To fabricate the NA sensor, 100 μL of 10 mM CD solution was dip-coated onto the retained area of $g\text{-C}_3\text{N}_4/\text{Cys}/\text{Au NRs}$ electrode for 20 min. After rinsed with double distilled water and dried in air, the modified electrode was immersed into the 100 μL of 50 μM Het solution to prevent the nonspecific binding. Subsequently, the prepared electrode was soaked in proper concentration of NA solution for 30 min and the electrode was indicated as GCE/ $g\text{-C}_3\text{N}_4/\text{Cys}/\text{Au NRs}/\text{CD}/\text{NA}$.

Results and discussion

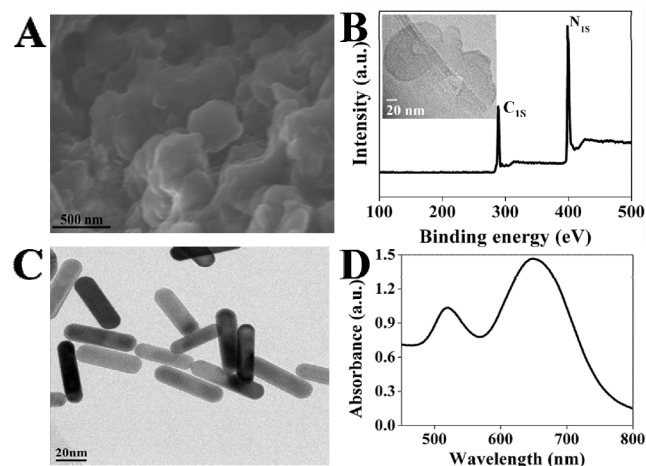


Fig. 1 SEM image (A) and XPS spectra (B) of $g\text{-C}_3\text{N}_4$ nanosheets. HRTEM image (C) and UV-vis Absorption spectra (D) of Au NRs. The inset in B is the HRTEM of $g\text{-C}_3\text{N}_4$.

Characterization of $g\text{-C}_3\text{N}_4$ and Au NRs

The SEM image of $g\text{-C}_3\text{N}_4$ was displayed in Fig. 1A, as it can be seen that the pure $g\text{-C}_3\text{N}_4$ sample was consisted of lamellar microscale particles with irregular sheets. Besides, the XPS of $g\text{-C}_3\text{N}_4$ (Fig. 1B) exhibited that the nanosheets were composed of carbon and nitrogen elements, and the successful preparation of $g\text{-C}_3\text{N}_4$ can be further certified by the Table S1 and the inset of Fig. 1B. As presented in Fig. 1C, Au NRs were well monodispersed and about cylindrical with hemispherical cap, and the length and width were approximately 40 nm and 9 nm, respectively, which the result is well in accordance with that of Fig. S1. The UV-vis absorption spectrum of Au NRs (Fig. 1D) showed two absorption peaks without any spectral broadening of the Plasmon bands, demonstrating that

the stability of Au NRs prepared in the work was very good, which in accordance with the result in Fig. S2. The emergence of weak and strong absorption peak correspond to the excitation of LSPR mode along the transverse and longitudinal directions, respectively.

Electrochemical and PEC behavior of g-C₃N₄/Cys/Au NRs

The electrochemical responses of the various modified electrodes in 5 mM K₃[Fe(CN)₆] solution containing 0.1 M KCl were recorded in Fig. 2A. Obviously, a classic pair of redox peaks was obtained at the GCE, whereas, the current decreased after g-C₃N₄ was deposited onto GCE which ascribed to the g-C₃N₄ impeded the transfer of electrons. It also demonstrated that g-C₃N₄ was successfully modified to the electrode. The current significantly diminished after the electrochemical polymerization of Cys at GCE/g-C₃N₄ as expected, owing to the Cys layer blocked the flow of a faradic current. Interestingly, the assembly of Au NRs to GCE/g-C₃N₄/Cys led to the recovery of well-defined redox peaks, and the corresponding electrochemical response was even as big as that of GCE. This phenomenon indicated that Au NRs possessed excellent conductivity and accelerated the transfer of electrons.

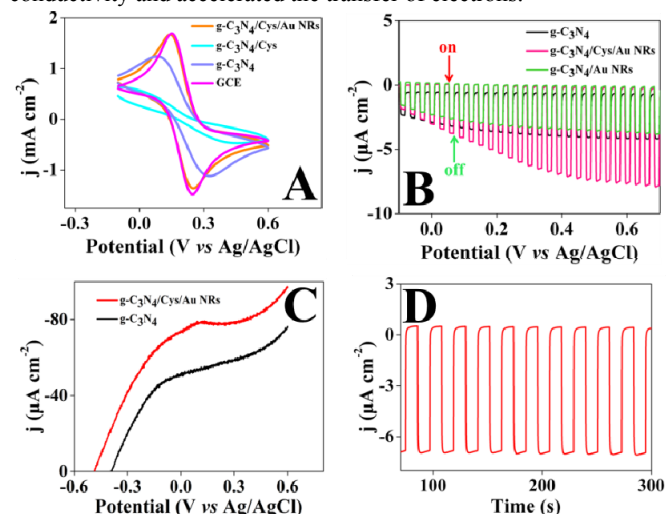


Fig. 2 (A) CV responses for different electrodes in 0.5 M KCl aqueous solution containing 10 mM K₃[Fe(CN)₆]. (B) The applied potential bias-dependent photocurrent densities of different modified electrodes in test solution. v : 5 mV s⁻¹ (C) The photocurrent density versus bias potential of different modified electrodes with the illumination of visible light. v : 0.1 V s⁻¹. (D) Photocurrent density of g-C₃N₄/Cys/Au NRs under visible light irradiation.

To investigate the PEC performance at different electrodes driven by visible light, the corresponding photocurrent densities were recorded in Fig. 2B. There was no photocurrent response detected on the bare GCE under the visible light induced (data not shown), whereas, a strong photocurrent was obtained on GCE/g-C₃N₄, indicating the g-C₃N₄ can function as an excellent photoactive material. Comparing g-C₃N₄, g-C₃N₄/Au NRs and g-C₃N₄/Cys/Au NRs modified electrodes, the photocurrent density of g-C₃N₄/Cys/Au NRs is largest at the entire potential window, which demonstrated Au NRs significantly improved the photocatalysis activity. However, the photocurrent densities of two former were almost equal, exhibiting that the Au NRs were not absorbed to GCE/g-C₃N₄ without the aid of Cys.

To further assess the photoelectrical performance of g-C₃N₄ and g-C₃N₄/Cys/Au NRs, LSV image and photo-conversion efficiency of them were recorded in Fig. 2C and Fig. S2. Two important conclusions can be concluded by analyzing the LSV data. One is that the photocurrent density of g-C₃N₄/Cys/Au NRs was higher in all applied biases in this study, demonstrating that the self-assembly of Au NRs is an effective mean for promoting the PEC performance of g-C₃N₄. The other is that the onset potential of g-C₃N₄/Cys/Au NRs (-0.49 V) was more negative than that of g-C₃N₄ (-0.39 V) and the photocurrent of g-C₃N₄/Cys/Au NRs saturated at a lower potential compared with that of g-C₃N₄. It is extraordinarily important for photosensitizer holding a low photocurrent onset and saturation potential because it can reduce the applied potential needed to obtain the maximum photocurrent, leading the enhancement of photoconversion efficiency, which is consistent with the result of the Fig. S2S. These findings support the earlier notion that Au NRs play an important role in improving the overall PEC performance.²⁶⁻²⁷ It is reasonable if taking into consideration of the synergic effect among g-C₃N₄ nanosheets and Au NRs, the detailed contributions from each component are currently being investigated.

The principle for enhanced photovoltaic performance of g-C₃N₄/Cys/Au NRs.

In this work, g-C₃N₄ as an n-type semiconductor, the Fermi level (E_F) is located at a more positive level than the lower edge of the conduction band (CB) but close to the conduction-band energy. As exhibited in Scheme 1B(a), the energy of CB (E_{CB}) in g-C₃N₄ is -1.13 eV (versus SHE) and the work function (W) of Au is 5.1 eV (0.66 eV versus SHE) higher than the electrochemical potential of O₂/H₂O₂ which is $E_{redox} = 0.68$ eV (versus SHE) before they contact. Owing to the available energy states in g-C₃N₄ and Au NRs are much fewer than those in solution because of the relatively small total surface areas, when the hybrid was contact with electrolyte solution, E_F and W changed significantly to line up with E_{redox} . Consequently, the electrons in the g-C₃N₄ were transported to the vacant level of Au NRs and holes were stored in g-C₃N₄, forming a built-in potential, Schottky barrier, in the depletion layer which in g-C₃N₄ near the interface (Scheme 1B (b)). Under the illumination of visible light in or near the depletion layer, the photoelectrons were driven to the CB of g-C₃N₄ and photoholes were expelled to Au NRs (then were efficiently scavenged by H₂O₂) by Schottky barrier. Thus the presence of Schottky barrier dramatically enhanced the separation of electrons and holes, significantly suppressed the recombination of photogenerated electron-hole pairs and greatly increased the photocatalytic performance of bare g-C₃N₄, which had demonstrated in Fig. 2B and Fig. 2C.

Furthermore, as elaborated in Scheme 1B (b), the electrons states in Au NRs were continuous and follow the Fermi-Dirac distribution under the dark.²⁸ Upon resonance with incidence photons (based on the LSPR effect) whose energy ($h\nu$) can overcome the top of bent conduction (E), many electrons would have higher energy than that of E_{CB} , facilitating a direct migration of electrons from Au NRs to CB of g-C₃N₄. As we all known, whatever the operate position (actual position) of the Fermi level after the contact, the gap between the Fermi level and the conduction-band top remains as $E = E_{CB} - E_F' = 0.68 - (-1.13) = 1.81$ eV. Undoubtedly, the LSPR-excited electrons

in Au NRs had sufficient energy to go across the depletion layer and flow into the CB of $g\text{-C}_3\text{N}_4$ because of the energy of the incident light in this study is 3.81 eV. Accordingly, the LSPR effect in the hybrid enhanced the absorption of visible light and generated more electrons, further improving the photocatalytic activity. To sum up, comparing with bare $g\text{-C}_3\text{N}_4$, these synergistic factors in $g\text{-C}_3\text{N}_4/\text{Cys}/\text{Au}$ NRs significantly increased photoelectrochemical responses by generating more carriers and accelerating the separation of photogenerated electrons and holes, which well explained the phenomena in Fig. 2B and Fig. 2C.

In addition, Au NRs can be used as a fascinating supported device and signal amplify element in biosensing, thus a variety of biological recognition systems can be designed based on this hybrid with outstanding PEC performance which motivated by the synergistic effect. Furthermore, under the optimal conditions (Fig. S5), the strong and stable photocurrent could reproducibly and drastically increased under irradiation and recovered quickly in the dark (Fig. 2D). Consequently, the high photovoltaic activity and good stability of $g\text{-C}_3\text{N}_4/\text{Cys}/\text{Au}$ NRs composite indicated that the $g\text{-C}_3\text{N}_4/\text{Cys}/\text{Au}$ NRs is desirable for designing high-performance PEC sensors.

Characterizing the fabrication process of the sensor

To evaluate the sensing application of aforementioned hybrid, NA, a principal substance of the flavonoid family, was selected as object for quantitative determination using PEC technique. NA has been proved to exhibit biological and pharmacological activity including potent anti-bacterial²⁹, anti-inflammatory³⁰, and anti-cancer³¹ effects. Thereby, it is significant to delve an accurate and rapid quantitative determination of NA. Herein, a tentative principle for the NA detection was proposed (Scheme 1). The introduction of Au NRs to $g\text{-C}_3\text{N}_4$ surface via Cys remarkably enhanced the photocurrent response. While the diffusion of H_2O_2 to electrode surface was inhibited by the assembled CD which resulted in increased recombination of photo-generated electron-hole pairs, leading the photocurrent density reduced. Then the photocurrent response further reduced after NA was specifically recognized by CD, owing to the increased resistance of the H_2O_2 diffusion. Therefore, NA can be successfully detected by taking the advantage of the dependence of the photocurrent signal change on the concentration of NA.

The construction process of the electrode was monitored by EIS. As demonstrated in Fig. 3A, the bare GCE exhibited a very small electron transfer resistance (curve a). After the $g\text{-C}_3\text{N}_4$ and Cys were modified onto the surface of bare GCE step by step, the diameter of the high frequency semicircle increased gradually, due to their low conductivity, indicating that the $g\text{-C}_3\text{N}_4$ and GCE/ $g\text{-C}_3\text{N}_4$ /Cys were successfully fabricated. Afterwards, the diameter (curve d) decreased after GCE/ $g\text{-C}_3\text{N}_4$ /Cys was immersed into Au NRs solution for 20 min because of the excellent electric conductivity of Au NRs, demonstrating the Au NRs were successfully assembled onto the surface of $g\text{-C}_3\text{N}_4/\text{Cys}/\text{GCE}$, which is well consistent with the results of Fig. S3 and S4. Besides, the shift of Au 4f peak by comparing the XPS of $g\text{-C}_3\text{N}_4/\text{Cys}/\text{Au}$ NRs with that of Au NRs also demonstrated the successful self-assembly of Au NRs (data not shown), which can be supported by pervious reports.³²⁻³³ While after CD (10 mM) was assembled to the Au NRs/Cys/ $g\text{-C}_3\text{N}_4$ modified electrode, the

resistance increased due to that CD acted as a barrier to the interfacial electron transfer. Finally, the resistance drastically augmented which was ascribed to that NA penetrated into the cavity of CD and formed an inclusion complex. These changes of diameters entirely manifested that the sensor was successfully fabricated, which is very consistent with the corresponding result from Fig. 3B. Besides, the stepwise photocurrent changes during the assembly of functionalized electrode in the “proof-of-principle” experiments (Fig. 3B) also confirmed the proposed hypothesis.

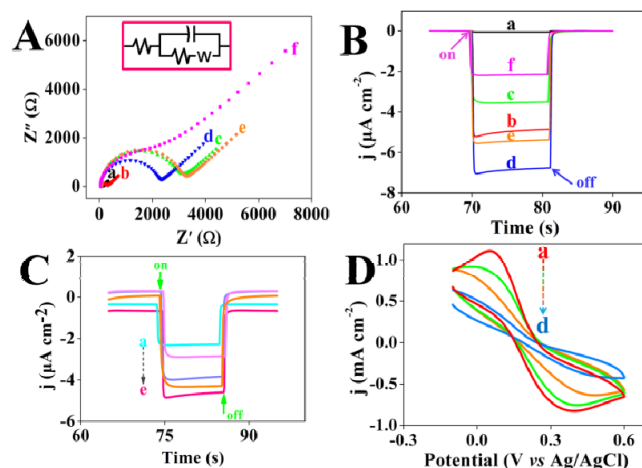


Fig. 3 (A) EIS and (B) Photocurrent densities of different electrodes: (a) GCE, (b) GCE/ $g\text{-C}_3\text{N}_4$, (c) GCE/ $g\text{-C}_3\text{N}_4/\text{Cys}$, (d) GCE/ $g\text{-C}_3\text{N}_4/\text{Cys}/\text{Au}$ NRs, (e) GCE/ $g\text{-C}_3\text{N}_4/\text{Cys}/\text{Au}$ NRs/CD, (f) GCE/ $g\text{-C}_3\text{N}_4/\text{Cys}/\text{Au}$ NRs/CD/NA. The inset in A shows the equivalent circuit. (C) Photocurrent densities of (a) GCE/ $g\text{-C}_3\text{N}_4/\text{Cys}/\text{Au}$ NRs/CD/NA, (b) GCE/ $g\text{-C}_3\text{N}_4/\text{Cys}/\text{Au}$ NRs/CD, (c) GCE/ $g\text{-C}_3\text{N}_4/\text{Cys}/\text{Au}$ NRs/NA, (d) GCE/ $g\text{-C}_3\text{N}_4/\text{Cys}/\text{Au}$ NRs in test solution and (e) GCE/ $g\text{-C}_3\text{N}_4/\text{Cys}/\text{Au}$ NRs in test solution containing 10 μM NA. (D) CV responses for (a) GCE/ $g\text{-C}_3\text{N}_4/\text{Cys}/\text{Au}$ NRs/CD and was self-assembled with 50 μM of (b) Mba, (c) Amp, and (d) Het in 0.5 M KCl aqueous solution containing 10 mM $\text{K}_3[\text{Fe}(\text{CN})_6]$.

Mechanism for the detection of NA

To further validate the proposed hypothesis and investigate the mechanism for the detection of NA in this work, the photocurrent responses of different electrodes were compared in Fig. 3C. By comparing curve c and e, the negligible change in photocurrent densities exhibited that there was no direct interaction between Au NRs and NA. As demonstrated by comparing the curve a, b and e, the photocurrent density decreased progressively when the CD (curve b) and NA (curve a) were assembled onto the surface of modified electrode step by step. The declined photocurrent was attribute to the CD was assembled onto the $g\text{-C}_3\text{N}_4/\text{Cys}/\text{Au}$ NRs and the NA can be specific recognized by CD which impeded the diffusion of redox to the electrode, accelerating the recombination of photogenerated electron-hole pairs, which is in accordance with the notion we proposed. Therefore, the quantitative determination of NA can be actualized according to the dependence of the photocurrent responses on the concentration of NA. Besides, the photocurrent of curve e was almost the same as that of curve d, thus the NA acted as electron-donor or electron-acceptor in this determination process could be excluded and the decreasing of photocurrent was attributed

to the specific recognized between CD and NA. The finding supports the aforementioned hypothesis.

Analytical performance

To explore the detection performance of the sensor, the photocurrent densities at various concentrations of NA were researched. As illustrated in Fig. 4A, under the optimum conditions (Fig. S6 and Fig. 3D), the photocurrent intensity decreased with the increasing of the NA concentration, which provided the basis for fabricating the PEC sensor to realize the detection of NA. As expected, the Δj increased with the increasing NA concentration and the dependence was linear with the logarithm value of NA concentration in the range from 1×10^{-4} to 1×10^{-10} M with a detection limit of 30 pM, which is outstanding compared with other reported previously (Table S2).³⁴

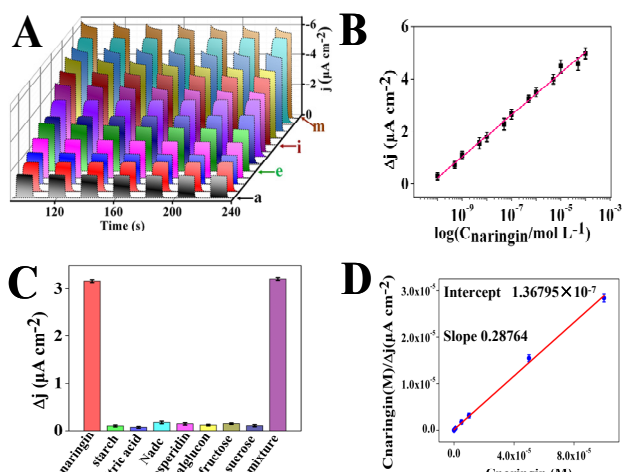


Fig. 4 (A) Photocurrent densities of GCE/g-C₃N₄/Cys/Au NRs/CD/Het was self-assembled with (a-m) 0.0001, 0.0005, 0.001, 0.005, 0.01, 0.05, 0.1, 0.5, 1, 5, 10, 50, and 100 μM of NA in test solution. (B) The corresponding calibration curve. (C) Selectivity of the PEC sensor to NA by comparing it to the interfering substances at the 1 mM level: starch, citric acid, calglucon, fructose, sucrose and 10 mM level: Nadc, hesperidin. (D) Linear regression between $C_{\text{NA}}/\Delta j$ and C_{NA} .

As manifested in the Fig. S7, the photocurrent density was highly stable under continuous light irradiation (curve a) and switching without observable deterioration, demonstrating good chemical and structural stability of the proposed sensor. Besides, no evident descend in the photocurrent was observed after two weeks of storage at 4 $^{\circ}\text{C}$, validating that the fabricated sensor possessed outstanding storage stability.

Three freshly prepared modified electrodes were tested under the same conditions to evaluate the reproducibility of the proposed sensor, all the electrodes displayed almost similar photocurrent response and the RSD of 3.7% was obtained, implying the sensor possess good fabrication reproducibility and detection precision.

In additional, the influence of NA analogues and some potential coexisting compounds were investigated under the same experimental conditions. Fig. 4C exhibited the photocurrent responses of these compounds almost no any great increase of photocurrent. Furthermore, the mixed sample did not display

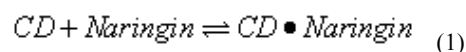
obvious photocurrent change compared with that of NA alone, suggesting the novel PEC sensor has high selectivity toward NA.

Analysis of real sample

To verify the feasibility of the sensor applied to practical samples, appropriate cough mixture without any pre-treatment expect to be diluted with ultrapure was analyzed. The result showed total amount of NA in the cough mixture was assessed to be $20.1 \mu\text{mol L}^{-1}$, which was consistent with $24.7 \mu\text{mol L}^{-1}$ obtained by using high performance liquid chromatography. Moreover, after different concentrations of standard NA were added into the above solution, the recovery of NA was in the range from 94.14% to 103.96% (Table S3), demonstrating this sensor can be successfully used for the monitor of NA in the piratical sample.

Inclusion Complexation of NA with CD

The real-time PEC sensing not only provides high sensitive determination for NA but also permits the direct measurement of binding constant between CD and NA. Clearly, after a g-C₃N₄/Cys/Au NRs/CD/Het modified electrode was immersed into NA solution, NA molecules were intercalated into the cavity of CD. Supposing the interaction process meets the requirements of Langmuir isotherm,³⁴⁻³⁵ the binding constant (K_b) can be expressed as follows:



$$K_b = \frac{[\text{CD} \bullet \text{NA}]}{[\text{CD}][\text{NA}]} \quad (2)$$

where $[\text{CD} \bullet \text{NA}]$, $[\text{CD}]$, $[\text{NA}]$ are the surface concentration of contacted CD•NA on the modified electrode, the concentration of CD on the g-C₃N₄/Cys/Au NRs/CD electrode, the concentration of NA solution, respectively. Thus, the relationship between photocurrent density change (Δj), the maximum photocurrent density change (Δj_{max} , $3.521 \mu\text{A cm}^{-2}$), the binding constant (K_b) and solution concentration of NA can be described as follows:

$$\Delta j = \frac{\Delta j_{\text{max}} \times K_b \times [\text{NA}]}{1 + K_b \times [\text{NA}]} \quad (3)$$

$$\frac{[\text{NA}]}{\Delta j} = \frac{1}{\Delta j_{\text{max}} \times K_b} + \frac{[\text{NA}]}{\Delta j_{\text{max}}} \quad (4)$$

As demonstrated in Fig. 4D, $[\text{NA}]/\Delta j$ versus $[\text{NA}]$ gave a straight line, which the intercept ($\Delta j_{\text{max}}^{-1} K_b^{-1}$) was 1.36795×10^{-7} and the slope ($\Delta j_{\text{max}}^{-1}$) was 0.28764. Consequently, $K_b = 2.076 \times 10^6 \text{ M}^{-1}$ was obtained, which is in accordance with that $3.978 \times 10^6 \text{ M}^{-1}$ in previous report, demonstrating that the exactness of the presumption and these equations, thus NA can be detected based on the PEC sensor.

Conclusion

In summary, we firstly developed a fascinating hybrid with enhanced photovoltaic performance by the synergistic effect of Schottky

1 barrier and LSPR based on multifunctional Au NRs decorated g-
2 C₃N₄. Then CD was used to assemble onto the surface of Au
3 NRs/Cys/g-C₃N₄ to fabricated a PEC biosensor for selectively and
4 effectively sensing for the first time due to that NA could permeate
5 into the cavity of CD and formed an inclusion complex which result
6 in the decreased of photocurrent. The outstanding features in this
7 detection including excellent selectively, high sensitivity, and wide
8 linear range demonstrated that the practical application can be
9 successfully realized based on this type PEC sensor. Therefore, the
10 first attempt to incorporate Au nanorods into graphitic-C₃N₄ to
11 enhance the photovoltaic performance by the synergic effect not
12 only provides new insights into the fabrication of light-sensitive
13 hybrid materials but also opens a new avenue for the applications of
14 plasmonic photocatalytic in photoelectrochemical sensing.

15 Acknowledgment

16 This project was financially supported by the NSFC (21205016), National
17 Science Foundation of Fujian Province (2011J05020), Education Department
18 of Fujian Province (JA14071, JB14036, JA13068) and Foundation of Fuzhou
19 Science and Technology Bureau (2013-S-113).

20 Notes and references

21 ^a College of Chemistry and Chemical Engineering, Fujian Normal University,
22 Fuzhou 350108, P. R. China, Fax: (+86)-591-22866135, E-mail:
23 dzhong@fjnu.edu.cn

24 ^b Ministry of Education Key Laboratory of Analysis and Detection for Food
25 Safety, and Department of Chemistry, Fuzhou University, Fuzhou 350002, P.
26 R. China

27 †Electronic Supplementary Information (ESI) available: Experimental;
28 Further analysis on photoconversion efficiency of the hybrid; TEM image
29 of g-C₃N₄/Cys/Au NRs hybrid; UV-vis absorption spectra of g-C₃N₄, Au
30 NRs and g-C₃N₄/Cys/Au NRs hybrid; Photocurrent changes during the
31 assembly of electrode and optimization of blocking agents; Control of
32 conditions in fabricating of PEC hybrid; Futhure analysis on Optimization
33 of detection condition; Table S1 Comparable figures of determining NA;
34 Table S2 The results of addition recovery test. See
35 DOI: 10.1039/b000000x/

- 36 1 Y. T. Long, C. Kong, D. W. Li, Y. Li, S. Chowdhury and H. Tian,
37 *Small*, 2011, **7**, 1624.
- 38 2 H. B. Li, J. Li, Q. Xu and X. Y. Hu, *Anal. Chem.*, 2011, **83**, 9681.
- 39 3 X. R. Zhang, Y. P. Xu, Y. Q. Yang, X. Jin, S. J. Ye, S. S. Zhang and
40 L. L. Jiang, *Chem.–Eur. J.*, 2012, **18**, 16411.
- 41 4 X. R. Zhang, S. G. Li, X. Jin, and S. S. Zhang, *Chem. Commun.*,
42 2011, **47**, 4929.
- 43 5 H. J. Shi, G. H. Zhao, M. C. Liu and Z. L. Zhu, *Electrochem.*
44 *Commun.*, 2011, **13**, 1404.
- 45 6 W. T. Sun, Y. Yu, H. Y. Pan, X. F. Gao, Q. Chen and L. M. Peng, *J.*
46 *Am. Chem. Soc.*, 2008, **130**, 1124.
- 47 7 Y. J. Zhang and M. Antonietti, *Chem. Asia J.*, 2010, **5**, 1307.
- 48 8 J. Q. Tian, Q. Liu, A. M. Asiri, A. O. Al-Youbi and X. P. Sun, *Anal.*
49 *Chem.* 2013, **85**, 5595.
- 50 9 N. Y. Cheng, P. Jiang, Q. Liu, J. Q. Tian, A. M. Asiri and X. P. Sun,
51 *Analyst*, 2014, **139**, 5065.
- 52 10 J. Q. Tian, Q. Liu, A. M. Asiri, A. H. Qusti, A. O. Al-Youbi and X. P.
53 Sun, *Nanoscale*, 2013, **5**, 11604.
- 54 11 Y. Wang, X. C. Wang and M. Antonietti, *Angew. Chem., Int. Ed.*,
55 2012, **51**, 68.

- 56 12 J. Q. Tian, Q. Liu, C. J. Ge, Z. C. Xing, A. M. Asiri, A. H. Qusti, A.
57 O. Al-Youbi and X. P. Sun, *Nanoscale*, 2013, **5**, 8921.
- 58 13 J. Q. Tian, R. Ning, Q. Liu, A. M. Asiri, A. O. Al-Youbi and X. P.
59 Sun, *ACS Appl. Mater. Inter.*, 2014, **6**, 1011.
- 60 14 Y. Zheng, J. Liu, J. Liang, M. Jaroniec and S. Z. Qiao, *Energy*
Environ. Sci., 2012, **5**, 6717.
- 1 X. F. Chen, J. S. Zhang, X. Z. Fu, M. Antonietti and X. C. Wang, *J.*
Am. Chem. Soc., 2009, **131**, 11658.
- 2 G. Liu, P. Niu, C. Sun, S. C. Smith, Z. Chen, G. Q. Lu and H. M.
Cheng, *J. Am. Chem. Soc.*, 2010, **132**, 11642.
- 3 S. X. Min and G. X. Lu, *J. Phys. Chem. C*, 2012, **116**, 19644.
- 4 A. Dawson and P. V. Kamat, *J. Phys. Chem. B*, 2001, **105**, 960.
- 5 V. Subramanian, E. E. Wolf and P. V. Kamat, *J. Phys. Chem. B*, 2003,
107, 7479.
- 6 J. S. Lee, E. V. Shevchenko and D. V. Talapin, *J. Am. Chem. Soc.*,
2008, **130**, 9673.
- 7 P. V. Kamat, *J. Phys. Chem. C*, 2008, **112**, 18737.
- 8 R. Costi, G. Cohen, A. Salant, E. Rabani and U. Banin, *Nano Lett.*,
2009, **9**, 2031.
- 9 D. V. Talapin, J. S. Lee, M. V. Kovalenko and E. V. Shevchenko,
Chem. Rev., 2010, **110**, 389.
- 1 N. Y. Cheng, J. Q. Tian, Q. Liu, C. J. Ge, A. H. Qusti, A. M. Asiri, A.
O. Al-Youbi and X. P. Sun, *ACS Appl. Mater. Interfaces.*, 2013, **5**,
6815.
- 2 Z. Wang, J. Liu and W. Chen, *Dalton Trans.*, 2012, **41**, 4866.
- 3 Y. C. Pu, G. M. Wang, K. D. Chang, Y. C. Ling, Y. K. Lin, B. C.
Fitzmorris, C. M. Liu, X. H. Lu, Y. X. Tong, J. Z. Zhang, Y. J. Hsu
and Y. Li, *Nano Lett.*, 2013, **13**, 3817.
- 4 J. Wang, S. L. Pan, M. Y. Chen and D. A. Dixon, *J. Phys. Chem. C*,
2013, **117**, 22060.
- 5 X. M. Zhang, Y. L. Chen, R. S. Liu and D. P. Tsai, *Rep. Prog. Phys.*,
2013, **76**, 046401.
- 6 G. K. Jayaprakasha, P. S. Negi, S. Sikder, L. J. Mohanrao and K. K.
Sakariah, *A: Phys. Sci.*, 2000, **55**, 1030.
- 7 S. Kawai, Y. Tomono, E. Katase, K. Ogawa and M. Yano, *Biosci.*,
Biotechnol., Biochem., 1999, **63**, 896.
- 8 V. S. Aboobaker, A. D. Balqi and R. K. Bhattacharya, *In Vivo.*, 1994,
8, 1095.
- 9 D. Barreca, A. Bovo, A. Gasparotto and E. Tondello, *Surf. Sci.*
Spectra, 2003, **10**, 21.
- 10 D. Barreca, A. Gasparotto, E. Tondello, G. Bruno and M. Losurdo, *J.*
Appl. Phys., 2004, **96**, 1655.
- 11 I. Langmuir, *J. Am. Chem. Soc.*, 1916, **38**, 2221.
- 12 I. Langmuir, *J. Am. Chem. Soc.*, 1918, **40**, 1361.